10-12-2015

Global patterns, trends, and drivers of water use efficiency from 2000 to 2013

Bao-Lin Xue
Chinese Academy of Sciences

Qinghua Guo
University of California at Merced

Alvarez Otto
University of California at Merced

Jingfeng Xiao
University of New Hampshire, Durham, j.xiao@unh.edu

Shengli Tao
Chinese Academy of Sciences

See next page for additional authors

Recommended Citation

Authors

Bao-Lin Xue, Qinghua Guo, Alvarez Otto, Jingfeng Xiao, Shengli Tao, and Le Li

Global patterns, trends, and drivers
of water use efficiency from 2000 to 2013

Bao-Lin Xue,[1] Qinghua Guo,[1,2,†] Alvarez Otto,[2] Jingfeng Xiao,[3] Shengli Tao,[1] and Le Li[1]

[1]State Key Laboratory of Vegetation and Environmental Change, Institute of Botany, Chinese Academy of Sciences,
No. 20 Nanxincun, Xiangshan, Beijing 100093 China
[2]School of Engineering, Sierra Nevada Research Institute, University of California at Merced, Merced, California 95343 USA
[3]Earth Systems Research Center, Institute for the Study of Earth, Oceans, and Space, University of New Hampshire,
Durham, New Hampshire 03824 USA

Abstract.   Water use efficiency (WUE; gross primary production [GPP]/evapotranspiration [ET]) estimates the tradeoff between carbon gain and water loss during photosynthesis and is an important link of the carbon and water cycles. Understanding the spatiotemporal patterns and drivers of WUE is helpful for projecting the responses of ecosystems to climate change. Here we examine the spatiotemporal patterns, trends, and drivers of WUE at the global scale from 2000 to 2013 using the gridded GPP and ET data derived from the Moderate Resolution Imaging Spectroradiometer (MODIS). Our results show that the global WUE has an average value of 1.70 g C/kg H_2O with large spatial variability during the 14-year period. WUE exhibits large variability with latitude. WUE also varies much with elevation: it first remains relatively constant as the elevation varies from 0 to 1000 m and then decreases dramatically. WUE generally increases as precipitation and specific humidity increase; whereas it decreases after reaching maxima as temperature and solar radiation increases. In most land areas, the temporal trend of WUE is positively correlated with precipitation and specific humidity over the 14-year period; while it has a negative relationship with temperature and solar radiation related to global warming and dimming. On average, WUE shows an increasing trend of 0.0025 g $C \cdot kg^{-1}$ $H_2O \cdot yr^{-1}$ globally. Our global-scale assessment of WUE has implications for improving our understanding of the linkages between the water and carbon cycles and for better projecting the responses of ecosystems to climate change.

† **E-mail:** guo.qinghua@gmail.com

INTRODUCTION

Water use efficiency (WUE) is the carbon uptake per unit water consumed by vegetation (g C/kg H_2O). It is an integrated physiological indicator and measures the tradeoff between carbon gain and water loss during photosynthesis (Farquhar et al. 1989, Cowan 2002). WUE is an important link of the carbon and water cycles, and improved understanding of its patterns and drivers is essential for the prediction of ecosystem responses to future climate change. For example, as a useful tool for water and carbon cycle simulation and prediction, WUE is used as an parameter in land surface or ecosystem models for the calculation of carbon assimilation in cases where evapotranspiration (ET) is known (Morén et al. 2001, Van Wijk and Bouten 2002,

Tang et al. 2006, Wang et al. 2014).

Theoretically, WUE should be the ratio of plant productivity to transpiration rather than to ET (the sum of evaporation from ground and canopy intercepted water and canopy transpiration). However, it remains a challenge to partition ET observations to plant transpiration and evaporation from soils and canopies (Baldocchi 2003, 2008). Therefore, the ratio of GPP to ET has been widely used to measure WUE (Yu et al. 2008, Xiao et al. 2013). Thus, WUE is typically calculated as the ratio of gross primary production (GPP) to ET, i.e., WUE = GPP/ET (e.g., Reichstein et al. 2007, Lu and Zhuang 2010, Mu et al. 2011*a*, Brümmer et al. 2012). An alternative definition of WUE is the ratio of net primary productivity (NPP) to ET (e.g., Dan and Ji 2007, Tian et al. 2011). The eddy covariance (EC) technique provides continuous measurements of net ecosystem exchange (NEE) and latent heat flux (or ET). NEE is routinely partitioned into GPP and ecosystem respiration. Therefore WUE, the ratio of GPP to ET, can be directly calculated from EC GPP and ET data.

Although a number of studies have assessed the patterns of WUE and its responses to climate (Niu et al. 2011, Linderson et al. 2012, Xiao et al. 2013), broad-scale research on WUE is limited mainly because of the lack of data (i.e., GPP and ET) at regional to global scales (Law et al. 2002, Reichstein et al. 2007, Beer et al. 2009, Keenan et al. 2013). Several studies examined the spatial patterns and controlling factors of WUE at regional or national scales using GPP and ET derived from EC flux towers (e.g., Beer et al. 2009, Keenan et al. 2013, Xiao et al. 2013) or process-based ecosystem models (e.g., Tian et al. 2010). Relatively few studies have assessed the magnitude, patterns, and trends of WUE at the global scale (Ito and Inatomi 2012).

Numerous studies have been conducted to investigate the influences of meteorological and morphological variables on WUE. Previous studies have examined the controlling effects of precipitation, temperature, solar radiation, and specific humidity (or vapor pressure deficit; Scanlon and Albertson 2004, Hu et al. 2008, Yu et al. 2008, Yang et al. 2010, Mu et al. 2011*a*). Several studies also examined the morphological effects of leaf area index (LAI) on WUE (Beer et al. 2009, Huang et al. 2010, Keenan et al. 2013).

However, the relative effects of these factors on WUE are not well understood. For example, Yu et al. (2008) found that WUE decreased with increasing precipitation for three forest sites in eastern China, whereas the opposite phenomenon was observed by Niu et al. (2011). A synthesis study by Keenan et al. (2013) showed that the meteorological variables had little effect on the increase in WUE at forest sites, and the main factor was increasing atmospheric CO_2 concentrations. The differences in these findings can be partly attributed to the different spatiotemporal scales, biomes, and locations of these studies.

Here we used a global GPP and ET dataset derived from MODIS over the period from 2000 to 2013 to assess the spatial patterns, trends, and drivers of WUE at the global scale. Specifically, we first examined the magnitude and spatial patterns of WUE. We then assessed the effects of morphological (LAI) and meteorological (precipitation, temperature, solar radiation, and specific humidity) drivers on WUE. We also assessed the interannual variability and trends of WUE over the 14-year period.

MATERIALS AND METHODS

GPP and ET data

We used the global GPP (Running et al. 2004, Zhao et al. 2005) and ET (Mu et al. 2007, 2011*b*) datasets derived from MODIS. The global GPP and ET datasets are both freely available on the Numerical Terradynamic Simulation Group website (http://www.ntsg.umt.edu). The MODIS GPP data (MOD17) are calculated as a multi-product function (Heinsch et al. 2003)

$$\text{GPP} = \varepsilon_{\max} \times 0.45 \times \text{SWrad} \times \text{FPAR} \times f\text{VPD} \times fT_{\min}$$

where $\varepsilon_{\max}$ is the maximum light use efficiency; SWrad is the short-wave downward solar radiation, of which 45% is photosynthetically active radiation (PAR); FPAR is the fraction of PAR absorbed by plants, which can be derived from MODIS products (MOD15A2, see below); fVPD and $fT_{\min}$ are the reduction scalars from water stresses (high daily vapor pressure deficit, VPD) and low temperature (low daily minimum temperature $T_{\min}$), respectively. The MOD17 GPP data were calculated globally at a 1-km resolution at 8-day, monthly (MOD17A2), and

annual (MOD17A3) intervals. A detailed description of the calculation of the MOD17 GPP can be found in Heinsch et al. (2003).

The MODIS ET product (MOD16) was produced by Mu et al. (2007, 2011b) based on the Penman–Monteith equation (Monteith 1964). At the global scale, MODIS land cover (MOD12Q1; Friedl et al. 2010), MODIS Collection 5 FPAR/LAI (MOD15A2; Myneni et al. 1997) and Collection 4 0.05-degree CMG MODIS albedo (Jin et al. 2003, Salomon et al. 2006) are used as the model inputs. The MODIS ET product is available globally at a resolution of 1 km. The improved version of annual MODIS ET products (MOD16A3) was used in this study and was downloaded from the Numerical Terradynamic Simulation Group website (ftp://ftp.ntsg.umt.edu/). The improved ET product is driven by a consistent version of meteorological variables from the GMAO (Global Modeling and Assimilation Office), and the ET was estimated with reasonable accuracy (Mu et al. 2011b).

In situ WUE database

We obtained in situ WUE values from the literature in order to evaluate the accuracy of the global WUE calculated from MODIS GPP and ET. Only sites with at least two years of data were selected because sites with one year of data generally did not cover the whole year. We obtained a total of 141 site years of WUE data from 34 flux tower stations (Appendix: Table A1). These sites encompass a range of ecosystems and climate types.

Land cover, elevation, LAI, and meteorological data

We used the global land cover map of MOD12Q1, which also has 1-km spatial resolution. As in Zhao and Running (2010), the University of Maryland (UMD) land cover classification scheme was used in our analysis. The UMD classification scheme consists of 11 biomes: evergreen needleleaf forest (ENF), evergreen broadleaf forest (EBF), deciduous needleleaf forest (DNF), deciduous broadleaf forest (DBF), mixed forest (MF), closed shrublands (CSH), open shrublands (OSH), woody savannas (WSA), savannas (SA), grasslands (GRA) and croplands (CRO).

We obtained elevation data from the NASA

Shuttle Radar Topographic Mission (SRTM) with a resolution of 1 km (http://srtm.csi.cgiar.org/). The LAI datasets are from MOD15A2 (https://lpdaac.usgs.gov/). To investigate the regression relationship between LAI and WUE on the annual scale, we calculated the average 8-day values within a year as a substitute for the annual average LAI.

The meteorological variables were obtained from the National Centers for Environmental Prediction, National Center for Atmospheric Research (NCEP-NCAR) Reanalysis II. The NCEP reanalysis dataset is freely available to the research community (Kanamitsu et al. 2002; http://www.esrl.noaa.gov/). The meteorological variables are available four times daily, and can be aggregated to daily, monthly, and annual time scales. These variables are in a Gaussian grid (T62, 192 × 94) projection and have a spatial resolution of $1.888° × 1.888°$ after spline interpolation. We resampled the NCEP data to 1-km resolution to match the spatial resolution of the GPP and ET data.

Data analysis

We used the MODIS GPP and ET to calculate WUE. For each 1-km grid cell, we calculated annual WUE from annual GPP and ET for each year over the period from 2000 to 2013; annual WUE values were then averaged over the 14 years to calculate mean annual WUE. Values above 1000 g C/kg H_2O were treated as abnormal and neglected throughout our research. We used the in situ WUE database to evaluate the accuracy of the global WUE dataset. It should be noted that there is scale mismatch for the comparison of in-situ and MODIS WUE values.

The interannual variability for the average 14-year WUE of each pixel was calculated using the bootstrap method (e.g., Zhang et al. 2013). The WUEs from the 14 observations were resampled 1000 times, and then the corresponding mean of each set of resampled data was calculated. Then, the 95% confidence limits for the resulting resampled data were calculated, and the width of the interval between the upper and lower limits was treated as the uncertainty level (at a 95% confidence level).

Regression analysis was conducted between WUE and different geographical (latitude and elevation), morphological (LAI), and meteoro-
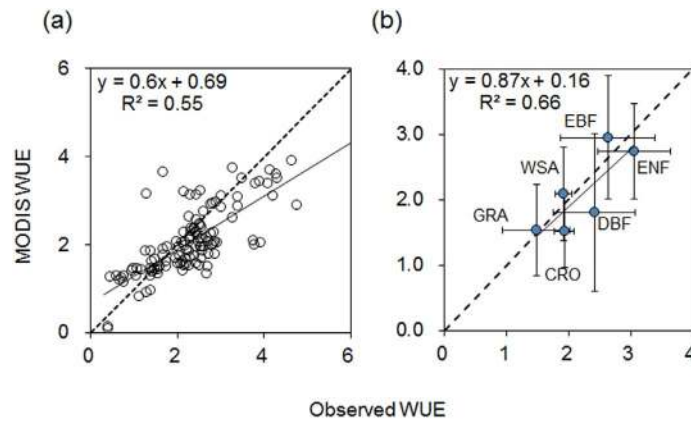
Fig. 1. Comparison of MODIS and observed water use efficiency (WUE, g C/kg H$_2$O) for (a) different sites and (b) averaged values of different biomes. The dash line shows the 1:1 line. The vegetation classification is based on the University of Maryland (UMD) scheme. The abbreviations are defined as follows: ENF, evergreen needleleaf forest; EBF, evergreen broadleaf forest; DBF, deciduous broadleaf forest; WSA, woody savannas; GRA grasslands; CRO, croplands. Error bars show the standard deviation of each biome for observed (horizontal) and MODIS-derived (vertical) values.

logical variables (precipitation, near surface air temperature [air temperature afterwards], downward short-wave solar radiation [solar radiation afterwards], and specific humidity). A specific analysis of the WUE according to different biomes was also conducted. The WUE trend was investigated by linear regression analysis. For each 1-km grid cell, we calculated the linear trend of WUE by regressing WUE against time.

RESULTS

Comparison of in situ and MODIS WUE data

We compared our global WUE dataset derived from MODIS GPP and ET data products against the eddy covariance (EC)-derived WUE database (Fig. 1a). There is a moderately strong relationship between the global WUE and EC-WUE ($R^2 = 0.55$, $p < 0.001$). Compared with EC values, the MODIS WUE slightly underestimated WUE for WUE values above 2 g C/kg H$_2$O and slightly overestimated WUE for WUE values below 2 g C/kg H$_2$O. This systematic error may be caused by the difference between the flux tower fetch and the MODIS resolution (Kim et al. 2012). Another reason may be that flux towers generally focus on high production ecosystems (Turner et al. 2006). It should also be noted that EC-calculated GPP is derived from the partitioning of net ecosystem exchange that often uses

empirical or process-based modeling (Desai et al. 2008). And therefore, Fig. 1 is not strictly a comparison of remote sensing to direct in situ observations.

The regression relationship much improves when we further compared at the biome level ($R^2 = 0.66$, $p < 0.001$). All of the biomes are scattered around the 1:1 line, except a relatively underestimated value for DBF (2.41 and 1.80 g C/kg H$_2$O for observed and MODIS estimated, respectively). Though observed WUE for CRO is larger than that for GRA, this value is also underestimated and is found be the least among all MODIS biomes (Fig. 1b).

Global patterns of WUE

Over the 14 years analyzed, the global average GPP and ET were 879.48 g C·m^{-2}·yr^{-1} and 518.83 mm/yr and this results in an average WUE of 1.70 g C/kg H$_2$O. WUE shows a large spatial variability at the global scale (Fig. 2). Large WUE values are found in humid and semi-humid areas of the northern hemisphere, such as Europe, central North America, and central and eastern Siberia, with relatively small interannual variations (Fig. 2b). WUE also shows large values in semi-arid areas, such as in the northern African savannas and open shrublands in southern South America and central Australia; however, WUE in these areas are with large interannual variations
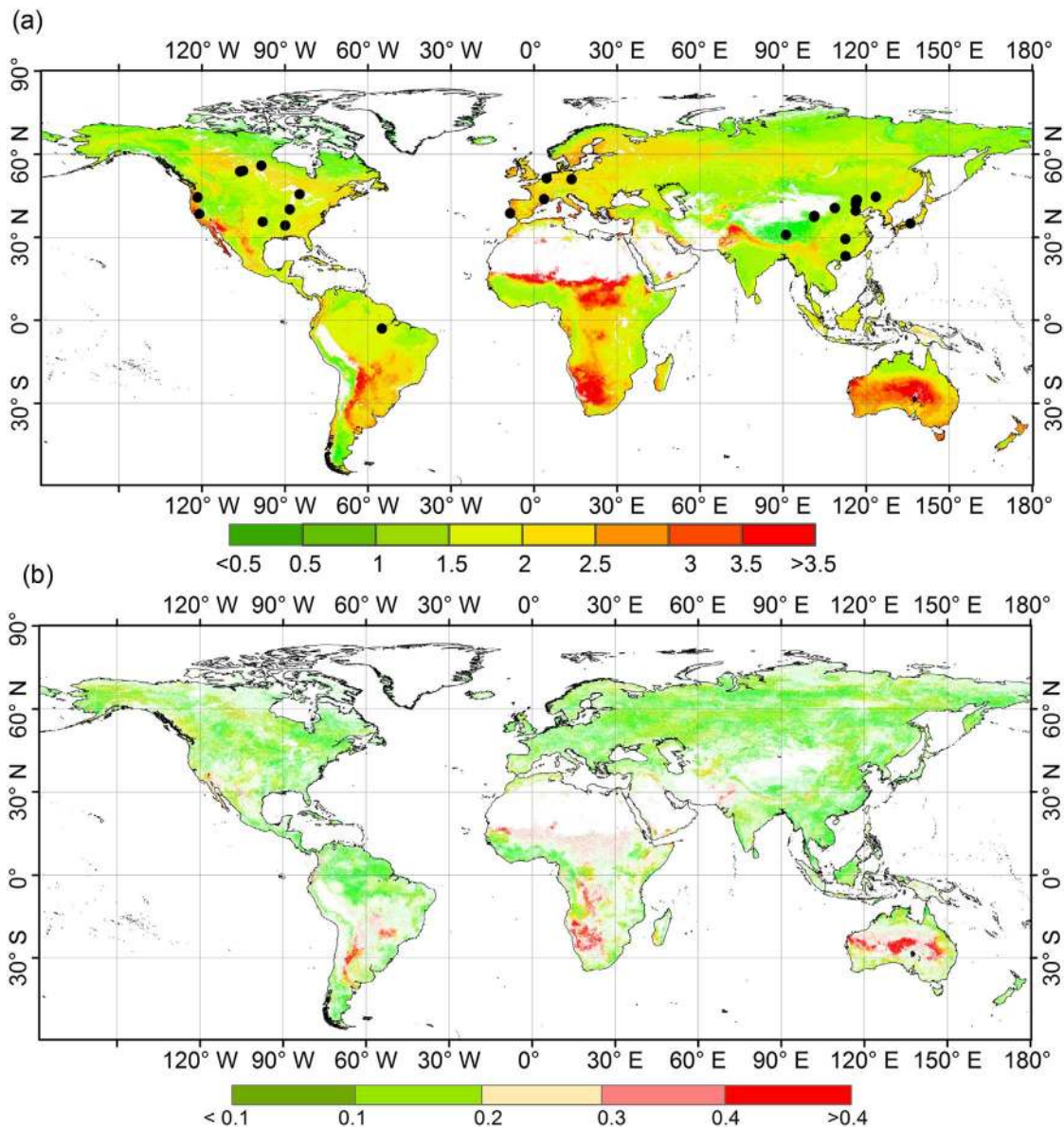
Fig. 2. (a) Spatial patterns of global water use efficiency (WUE, g C/kg H_2O) calculated as gross primary production (GPP)/evapotranspiration (ET); (b) interannual variability in WUE. The global WUE is calculated as the 14-year average from 2000 to 2013. The points in panel (a) show the validation sites from published literatures. The internal variability was calculated by bootstrap method and the results shown are within 95% confidence intervals. A large value shows large interannual variation of WUE in panel (b).

(Fig. 2b). In tropical areas such as the Amazonian Plain, central Africa, and Southeast Asia, the WUE shows moderate values with relatively small interannual variation. In contrast, the WUE values are small in areas with harsh meteorological conditions and less vegetation, such as the Arctic and Tibetan Plateau.

WUE is significantly different among biomes (one-way ANOVA, $\alpha = 0.05$; Fig. 3). In general, forests have the largest WUE among all biomes; closed shrublands also have relatively large WUE values but with large uncertainty; Croplands
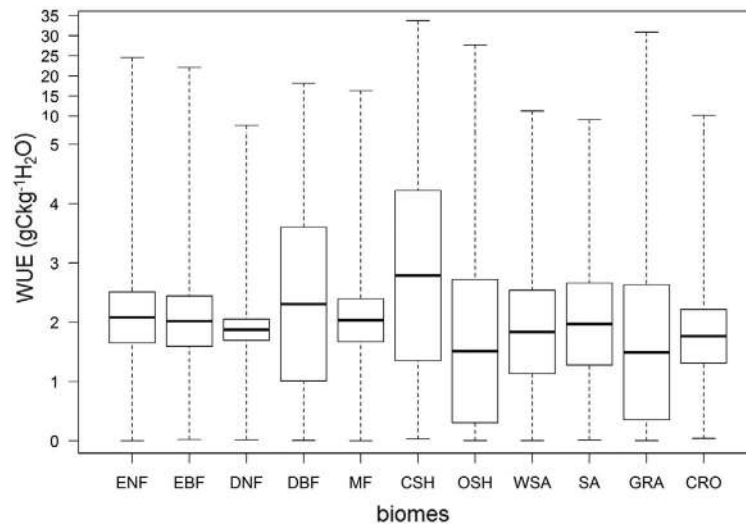
Fig. 3. Average WUE values for different biomes. The vegetation classification is based on the University of Maryland (UMD) scheme. The abbreviations are defined as follows: ENF, evergreen needleleaf forest; EBF, evergreen broadleaf forest; DNF, deciduous needleleaf forest; DBF, deciduous broadleaf forest; MF, mixed forest; CSH, closed shrublands; OSH, open shrublands; WSA, woody savannas; SA, savannas; GRA, grasslands; CRO, croplands. The band within a box shows the average WUE of each biome; the top and bottom of the box show the standard deviation of WUE and the ends of the whiskers show the minimum and maximum. The outliers are neglected in the figure. Each biome is significantly different from others (one-way ANOVA, $\alpha = 0.05$).

have intermediate values; grasslands have the lowest WUE (1.49 g C/kg H_2O). Among all forest types, deciduous broadleaf forest has the largest WUE, 2.31 g C/kg H_2O.

WUE is relatively stable as the elevation increases from 0 to 1100 m, and then rapidly decreases at higher elevations (Fig. 4). A maximum of 1.97 g C/kg H_2O is found at an elevation of 1105 m. WUE has a strong, negative relationship with elevation for elevation between 1105 and 5000 m (WUE $= -0.0004$ [elevation] $+ 2.34$, $R^2 = 0.94$, $p < 0.001$). Above 5000 m, the WUE is close to zero.

Globally, WUE varies much with latitude, especially for the southern hemisphere (Fig. 4). WUE begins to increase at ~$-50.5°$ S and reaches a maximum of 3.21 g C/kg H_2O at ~$-26.5°$ S. After a sharp decrease, the WUE is relatively stable between $-17.5°$ S and $60°$ N except extreme large values are found between $8.5°$ N and $18.5°$ N. The particularly high WUE values (above 3 g C/kg H_2O) found at around $-26.5°$ S and $16.5°$ N are caused by the large values in parts of Africa, Australia, and New Zealand (Fig. 2). The WUE values around these two latitudes are with large

uncertainty due to sparse vegetation. Above $60°$ N, the WUE decreases sharply with latitude (WUE $= -0.075$ [latitude] $+ 6.153$, $R^2 = 0.98$, $p < 0.001$).

The morphological effects of vegetation on WUE were assessed using the LAI. The global average LAI varies from 0 to 8.7 m^2/m^2 at the annual scale over the study period (Fig. 5). The WUE first linearly increases sharply when the LAI is smaller than 1.5 m^2/m^2 (WUE $= 0.172$ [LAI] -0.281, $R^2 = 0.98$, $p < 0.001$) with a maximum of 2.26 g C/kg H_2O. After decreases through 2.1 m^2/m^2, WUE starts to increase from 1.75 to 2.14 g C/kg H_2O when LAI reaches 4.8 m^2/m^2 (WUE $= 0.014$ [LAI] $+ 1.43$, $R^2 = 0.97$, $p < 0.001$). When LAI is above 4.8 m^2/m^2, WUE does not fluctuate much.

Effects meteorological drivers on spatial patterns of WUE

Two maxima of (2.72 and 2.64 g C/kg H_2O) are observed in extremely dry and wet areas with large uncertainties. The WUE first increases as precipitation increases when the latter is below 2353 mm/yr (WUE $= 0.0001$ [precipitation] $+ 1.61$,
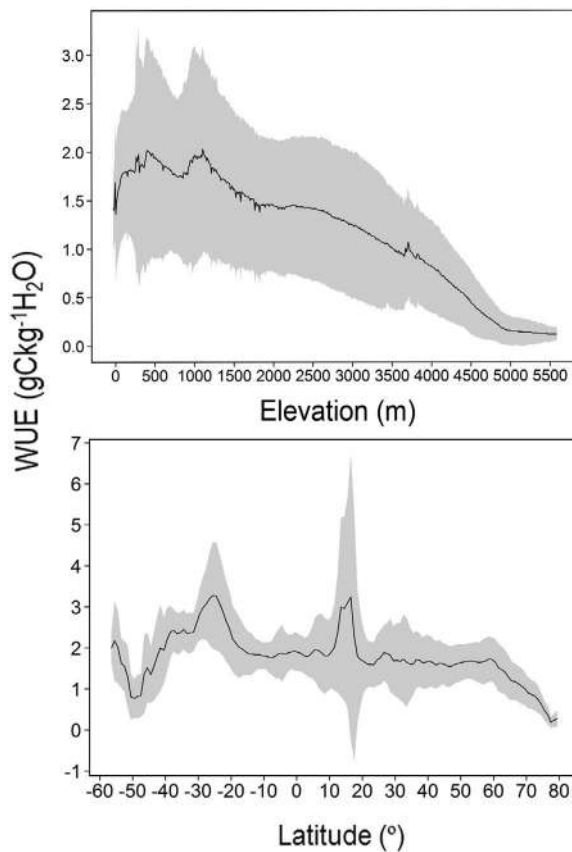
Fig. 4. Altitudinal and latitudinal WUE patterns. Altitude is from DEM (m) values. Each point represents averaged WUE values for 100 m and 1° intervals for altitude and latitude, respectively. Gray zones show the standard deviation of each interval.

Fig. 5. Morphological WUE patterns as represented by leaf area index (LAI). Each point represents averaged WUE for 0.1 m^2/m^2 intervals of LAI. Gray zones show the standard deviation of each interval.

$R^2 = 0.50$, $p < 0.001$); while it decreases when precipitation is above this value until precipitation is around 4450 mm/yr (WUE = −0.0002 [precipitation] + 2.31, $R^2 = 0.40$, $p < 0.001$) (Fig. 6a). WUE also shows large variations with temperature changes (Fig. 6b). In regions where the temperature is below 20°C, WUE tends to increase as the temperature increases by a linear relationship (WUE = 0.054 [temperature] + 1.33, $R^2 = 0.85$, $p < 0.001$) and reaches a maximum of 3.51 g C/kg H_2O at ~18.5°C. WUE then decreases sharply until 25.7°C (WUE = −0.0997 [temperature] + 4.50, $R^2 = 0.51$, $p < 0.001$) and shows extremes values with large uncertainty afterwards.

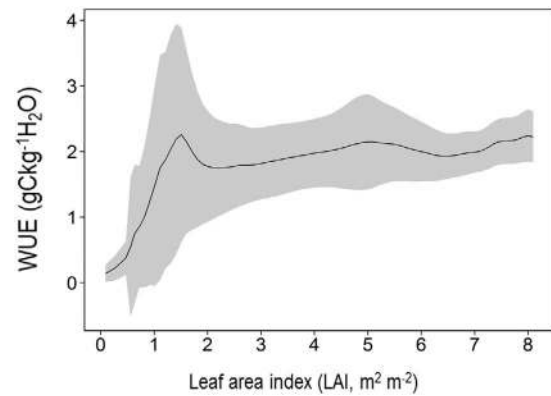The WUE increases as the solar radiation increases in regions where solar radiation is less than 242.2 W/m^2 (WUE = −0.009 [solar radiation] + 0.023, $R^2 = 0.83$, $p < 0.001$; Fig. 6c). The WUE reaches a maximum of 2.65 g C/kg H_2O at ~242.2 W/m^2 and tends to decrease as solar radiation increases (WUE = −0.032 [solar radiation] +10.193, $R^2 = 0.85$, $p < 0.001$). Since the solar radiation for most land areas (90%) is below 242.2 W/m^2, this indicates a large solar radiation would introduce a large WUE in most land areas. WUE also changes with specific humidity (Fig. 6d). In relatively dry regions where specific humidity is less than 0.0072 kg/kg, WUE is larger when the specific humidity is large (WUE = 392.92 [specific humidity] −0.3, $R^2 = 0.99$, $p < 0.001$). WUE reaches its maximum of 2.24 g C/kg H_2O around 0.0092 kg/kg and then becomes stable when specific humidity is above 0.01 kg/kg.

Trends in WUE

From 2000 to 2013, GPP, ET, and WUE show relatively large variations at the global scale (Table 1). The maximum GPP occurs in 2013, with a value of 901.13 g C·m^{-2}·yr^{-1}. The minimum GPP is observed in 2002, with a value of 860.41 g C·m^{-2}·yr^{-1}. The maximum and minimum ET values are observed in 2010 and 2002 as 530.2 and 511.66 mm/yr, respectively. The maximum and minimum WUE values are observed as 1.75 and 1.66 g C/kg H_2O in 2013 and 2010, respectively. The GPP shows an increasing trend over the 14-year period ($R^2 = $
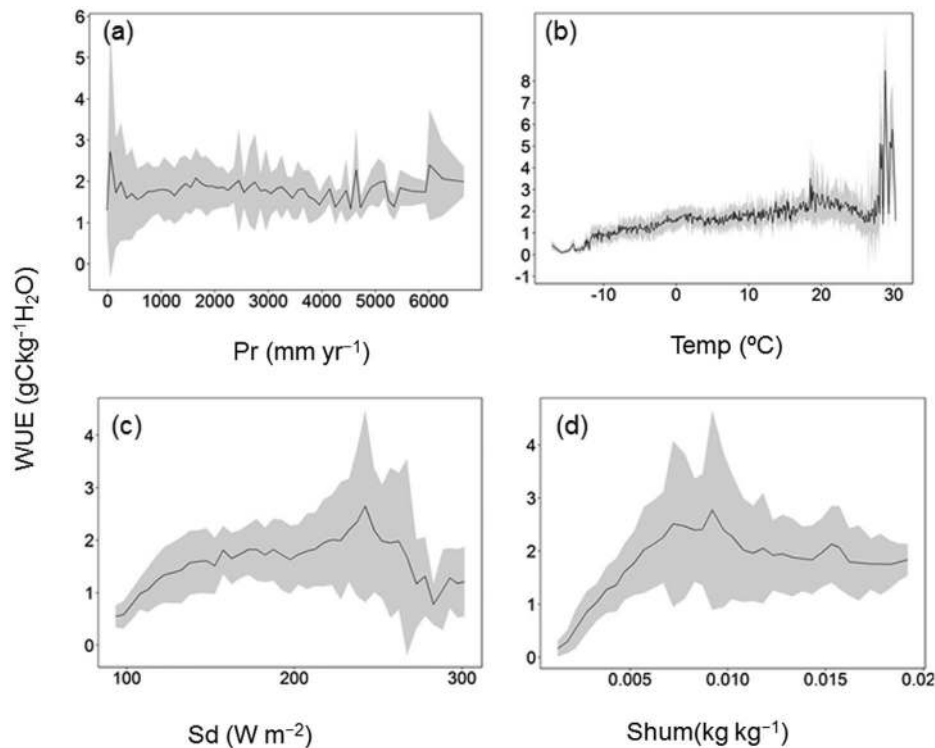
Fig. 6. WUE patterns with (a) precipitation (Pr, mm/yr), (b) temperature (Temp, °C), (c) solar radiation (Sd, W/m^2), and (d) specific humidity (Shum, kg/kg). Each point represents averaged WUE for 100 mm/yr, 0.5°C, 5 W/m^2, and 0.001 kg/kg intervals for precipitation, temperature, solar radiation, and specific humidity, respectively. Gray zones show the standard deviation of each interval.

0.71, $p < 0.01$), but no significant trend is observed for ET ($p = 0.12$). This results in an increasing trend in WUE ($p = 0.12$). Therefore, WUE is more influenced by GPP than by ET over the study period.

Overall, WUE increases by 0.0025 g C·kg^{-1} H$_2$O·yr^{-1} at the global scale (Fig. 7a). Areas with a positive trend in WUE account for 58% of the global land area. WUE increases rapidly in almost the entire North America and a highly significant increase is observed in Alaska (Fig. 7b). Positive trends are also found in the Amazonian Plain, central Africa, India, and eastern China. These areas show relatively large WUE values and large positive trends. In contrast, in Eastern Europe, northern Africa, and southern South America, where large WUE values are found (Fig. 2), large deceasing trends are observed (Fig. 7b).

Significant increasing trends are observed for evergreen needleleaf forest ($R^2 = 0.34$, $p = 0.02$), closed shrublands ($R^2 = 0.49$, $p = 0.01$), open

shrublands ($R^2 = 0.66$, $p < 0.001$), and woody savannas ($R^2 = 0.30$, $p = 0.04$; Fig. 8). In contrast, no significant trends are observed for other biomes. The four biomes with increasing trends

Table 1. Global average gross primary production (GPP), evapotranspiration (ET), and WUE (=GPP/ET) from 2000 to 2013.

Year	GPP (g C·m^{-2}·yr^{-1})	ET (mm/yr)	WUE (g C/kg H$_2$O)
2000	870.95	515.43	1.690
2001	872.13	512	1.703
2002	860.41	511.66	1.682
2003	874.79	516.41	1.694
2004	877.30	516.69	1.698
2005	866.99	514.08	1.686
2006	877.92	523.08	1.678
2007	882.57	528.68	1.669
2008	876.78	520.68	1.684
2009	878.67	521.85	1.684
2010	880.35	530.2	1.660
2011	898.19	522.91	1.718
2012	894.59	514.52	1.739
2013	901.13	515.43	1.748
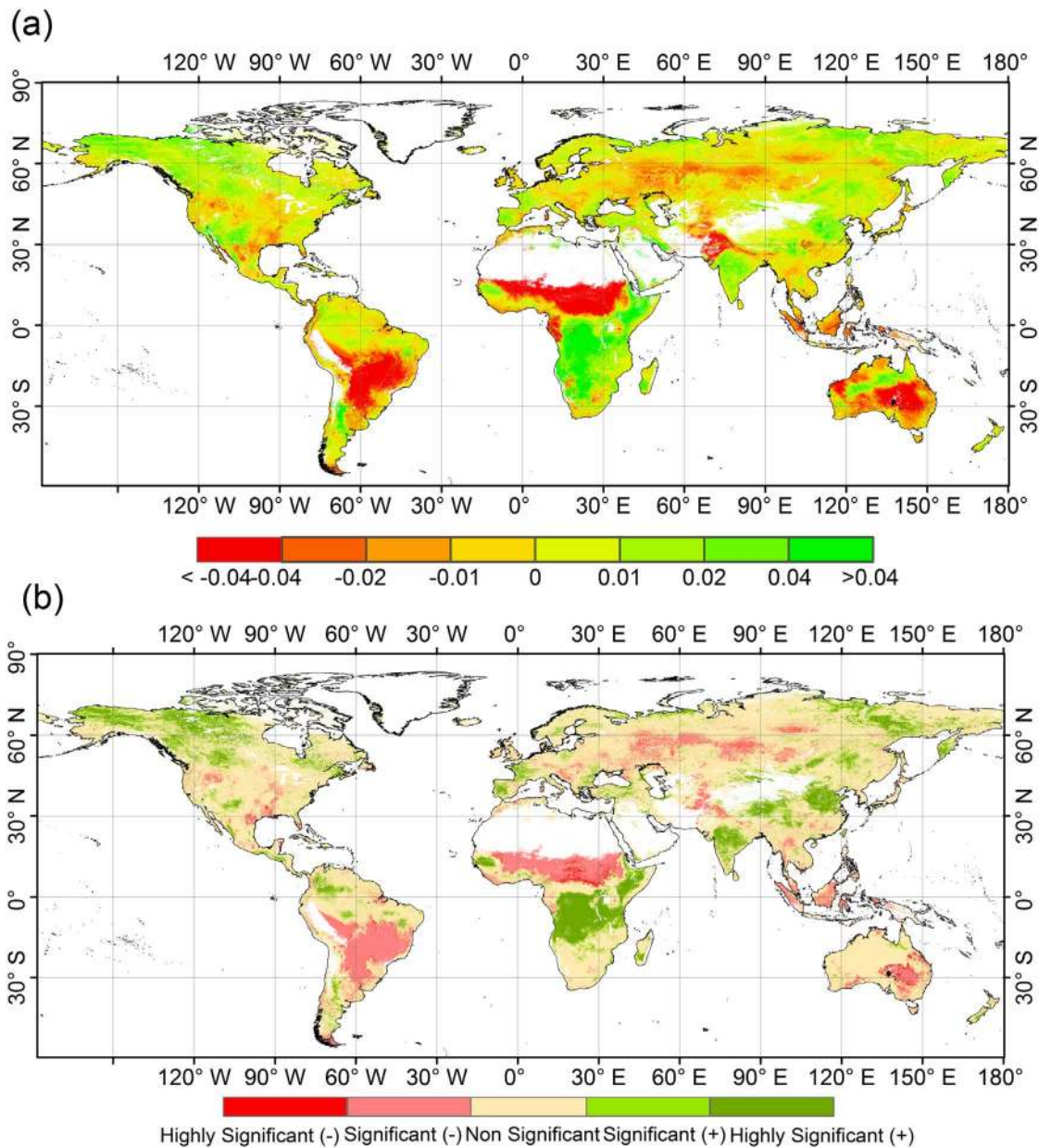
Fig. 7. Spatial patterns of (a) WUE trends (g C·kg^{-1} H$_2$O·yr^{-1}) from 2000 to 2013 and (b) significance of the trends. Highly significant (+), significant (+), non-significant, significant (−), and highly significant (−) show positive trend with $p < 0.05$, positive trend with $p < 0.1$, non-significant trend, negative trend with $p < 0.1$, and negative trend with $p < 0.05$ (t test).

explain the positive trends in most of the land surface areas (Fig. 7). Evergreen needleleaf forest, shrublands, and woody savannas occupy nearly 50% (7.4%, 31.0%, and 8.4%, respectively) of the total vegetated areas, and thus have essential roles in global WUE trends.

Effects of meteorological drivers on temporal trends in WUE

On average, precipitation increased by 6.44 mm yr/yr over the 14 years. In total, around 55% of the land surface experienced a positive trend (Appendix: Fig. A1). A positive linear relation-
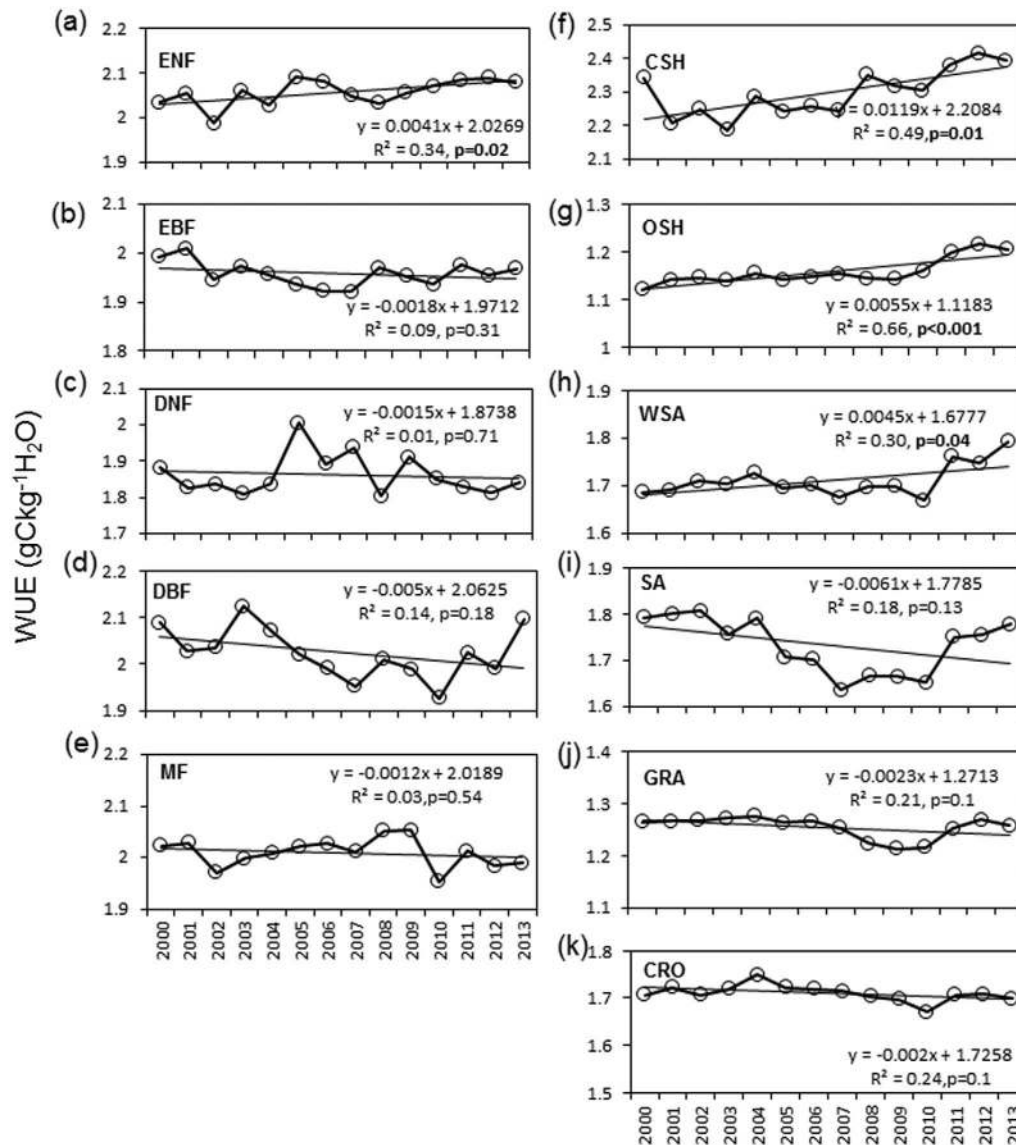
Fig. 8. Temporal trends in WUE for different biomes. The abbreviations for the different biomes are the same as those in Fig. 3. R^2 and p values are also shown.

ship is found between WUE and precipitation for 44% of the land surface, with an average slope of 0.0002 g C·kg^{-1} H$_2$O·mm^{-1}·yr (Fig. 9a). The positive relationship is found in areas with relatively dense vegetation (e.g., forests) and high precipitation; while the sparsely vegetated areas such as Northern Africa and northern Asia experience a negative relationship. Most of these sparsely vegetated areas have relative low precipitation (Appendix: Fig. A1). This indicates that WUE increases as precipitation increases in

relatively wet areas and increases as precipitation decreases in relatively dry areas.

Temperature increased over most parts of the global land surface (around 64%) during the study period with an average slope of 0.023° C/yr (Appendix: Fig. A2). Forty percent of the land area shows a negative relationship between WUE and temperature, with an average slope of −0.026 g C·kg^{-1} H$_2$O·°C^{-1} (Fig. 9b). The negative relationship is even more apparent for the southern hemisphere (SH), with high signifi-
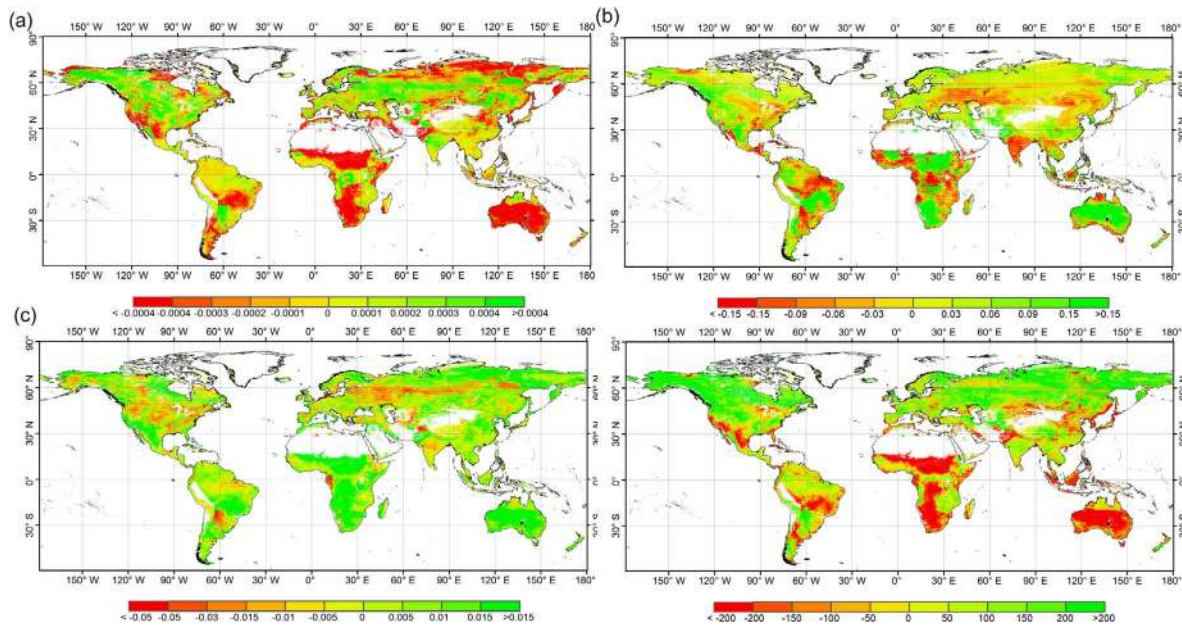
Fig. 9. Spatial patterns of regression slope between WUE and (a) precipitation, (b) temperature, (c) solar radiation and (d) specific humidity from 2000 to 2013. The regression relationship between meteorological variables and WUE is written as: [WUE] = a × [meteorological variable] + b, where a and b are regression coefficients.

cance. In the northern hemisphere, India and southern North America also show a negative relationship between WUE and temperature. However, for cold areas, such as the northern high latitudes and the Tibetan Plateau, a positive relationship is observed between WUE and temperature.

Over the 14 years, the global land surface experienced a dimming phase, with solar radiation decreasing by 0.15 $W \cdot m^{-2} \cdot yr^{-1}$ on average. Areas with decreasing trends occupy 57% of the total land surface (Appendix: Fig. A3). These areas are the same as those with increasing trends in precipitation, such as the Amazonian Plain, central and North Africa, and Southeast Asia, with high significance. Overall, solar radiation has a negative relationship with WUE trend for the global dimming, with an average slope of −0.005 g $C \cdot kg^{-1}$ $H_2O \cdot m^2 \cdot W^{-1}$ (Fig. 9c). This indicates that for most areas (around 67%), WUE increases as solar radiation decreases (Appendix: Fig. A3).

Not surprisingly, the specific humidity shows an increasing trend because of increasing precipitation at the global scale (0.00002 $kg \cdot kg^{-1} \cdot yr^{-1}$;

Appendix: Fig. A4). Areas with a positive trend account for 69% of the total land surface and the total area is a little larger than that for precipitation (Appendix: Fig. A4). WUE shows a positive relationship with specific humidity for 69% of the total land surface, and the average slope is 17.36 g $C \cdot kg^{-1}$ $H_2O \cdot kg \cdot kg^{-1}$ (Fig. 9d). In contrast, a significant negative relationship between WUE and specific humidity is observed in Southeast Asia, northern and southern Africa, and patchy areas in South America.

DISCUSSION

Global patterns and trends of WUE

WUE values generally show large spatial variability at the global scale. Generally, biomes with high productivity have large WUE values (Fig. 2a). In areas with sparse vegetation, a large WUE has also been observed but with large interannual variation (Fig. 2b). This is obvious for the WUE of CSH, which has a larger standard deviation compared with other biomes (Fig. 3). The negative relationship between WUE and elevation may also be caused by frequent ice and

snow cover and thus sparse vegetation associated with low temperature and precipitation in high-elevation areas (Fig. 4). The latitudinal WUE pattern clearly shows the influence of interannual variability induced by the sparse vegetation (Fig. 4).

The temporal trend over the 14 years studied varies greatly in magnitude and also differs in direction (increasing or decreasing). Few studies have examined global WUE (Dan and Ji 2007, Mu et al. 2011a, Ito and Inatomi 2012). Ito and Inatomi (2012) calculated WUE as NPP/ET or GPP/ET ratios using a global terrestrial model. They found that for the period 1995–2004, the global average WUE, calculated as GPP/ET, was 1.92 g C/kg H_2O, which is slightly higher than our value (1.70 g C/kg H_2O). This might be caused by the markedly larger WUE values for croplands and savannas in their results, and the different time period used. However, the spatial patterns obtained by Ito and Inatomi (2012) and by us are similar (Fig. 4 in Ito and Inatomi 2012). We further compare the WUE in the year of 2010 from our study with global WUE (Xiao et al., *unpublished manuscript*) calculated using a data-driven approach (Xiao et al. 2008) and WUE from Jung et al. (2011; Fig. 10a). WUE from Jung et al. (2011) is calculated as the ratio of GPP to ET and is scaled up from flux tower values by a machine learning technique for 2000–2011 at 0.5° × 0.5° grid resolution. We compare the biome-averaged WUE from the two studies. All the biomes are scattered around the 1:1 line except for closed shrublands (CSH) for both cases. WUE for CSH from our study (2.79 g C/kg H_2O) is much larger than those from Xiao et al. (*unpublished manuscript*) and Jung et al. (2011; 1.31 and 1.21 g C/kg H_2O, respectively). Since CSH occupies 0.5% of the global land area according to the MODIS land cover with the UMD classification scheme, we thus removed it from our figure. The regression relationship is much improved when CSH is removed (Fig. 10a). Note that WUE from our study is comparable with Xiao et al. (*unpublished manuscript*) for low productivity biomes and is smaller for high productivity biomes; while it is opposite when compared with Jung et al. (2011). At the global scale, the WUE patterns are similar among the three studies (Appendix: Fig. A5). WUE from Xiao et al. (*unpublished manuscript*) is largest for forests in

North America and Northern Asia (most above 2.5). Our estimates are between the estimates of the two datasets for these areas. However, WUE in Amazonia tropical forest from our results are systematically smaller than those of the other two studies (Appendix: Fig. A5). This might be caused by the smaller GPP from this area as MODIS GPP tends to be underestimated for the high-productivity ecosystems (Turner et al. 2006). A large positive bias is also observed for southern Arica and wet Australia, indicating large uncertainties for these areas (Fig. 2b). These results indicate necessity of validation of MODIS products of GPP and ET in more areas besides North America and Europe (Zhao et al. 2005, Mu et al. 2007).

Overall, an increasing trend is found during the research period on the global scale. These results are consistent with those of Ito and Inatomi (2012) and Dan and Ji (2007). Similarly, Tian et al. (2010) investigated WUE values (calculated as NPP/ET), using a process-based model, for the southern USA during 1895–2007. They found that WUE increased by 25% over the period for their study area. In contrast, our results show that several areas such as southern South America, Eastern Europe, and southern China show strong decreasing trends, which may be caused by climatic variables (Fig. 9).

Since the time period of our analysis based on the MODIS data is relatively short, we further compare the MODIS-derived WUE with that from the Integrated Biosphere Model (IBIS, Kucharik et al. 2000) and that from Jung et al. (2011; Fig. 10b). IBIS is run for the period 1948–2010 to calculate the global GPP and ET at 0.5° × 0.5° latitude–longitude grid resolution. Temporal trend of Jung et al. (2011) is for the period of 1982–2011 based on the available satellite data. WUE from IBIS shows a significant increasing trend for its analyzed period ($p < 0.001$); while it is not the case for Jung et al. (2011; $p = 0.19$). However, when evaluated for the period of 2000–2010 and 2000–2011 for IBIS and Jung et al. (2011), both of the two studies show significant increasing trends ($p = 0.009$ and $p = 0.045$ for IBIS and Jung et al. [2011], respectively). These results indicate that MODIS products can detect the disturbances and thus variations of WUE over the global scale. On the other hand, the absolute values of IBIS derived WUE are signif-
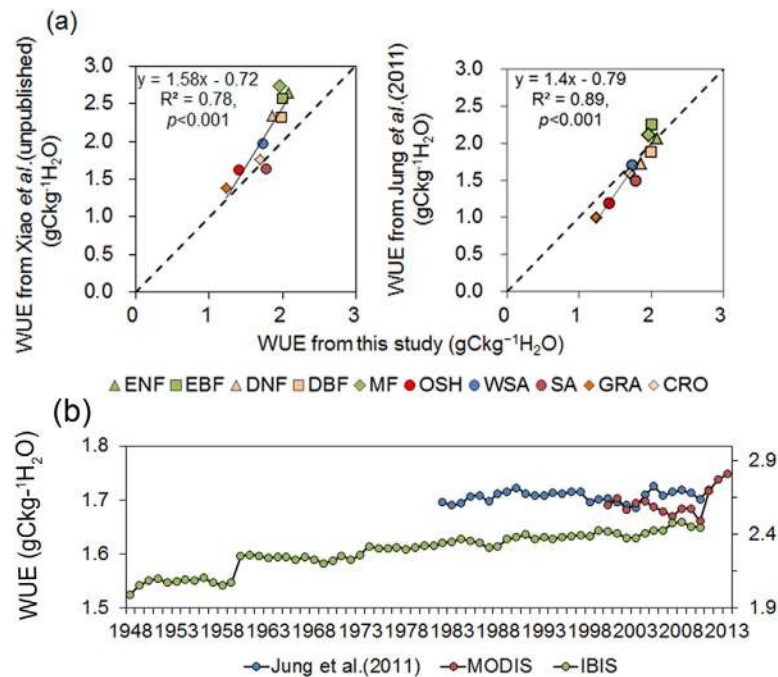
Fig. 10. (a) Comparison of biome-averaged WUE in 2010 from Xiao et al. (*unpublished manuscript*; left panel) and Jung et al. (2011; right panel) with that from our study; (b) comparison of time series of WUE from Jung et al. (2011), our study (MODIS) and that from the Integrated Biosphere Model (IBIS, right bar). The time period for Jung et al. (2011) and IBIS is 1982–2011 and 1948–2010, respectively. The abbreviations for the different biomes are the same as those in Fig. 3.

icantly larger than those from Jung et al. (2011) and MODIS products (one-way ANOVA, $p < 0.001$). This necessitates further work on the MODIS products validation or model calibration for GPP or ET accuracy assessments.

Influences of meteorological and morphological variables on WUE

The influences of meteorological and morphological variables on the patterns and trends of WUE, and the responses of WUE to these variables, may be different, or even opposite, at different spatial (leaf, canopy, ecosystem, regional, or global) and temporal scales (half-hourly, seasonal, and interannual; Scanlon and Albertson 2004, Krishnan et al. 2006, Hu et al. 2008, Yu et al. 2008, Tian et al. 2010, Yang et al. 2010, Mu et al. 2011a, Niu et al. 2011, Keenan et al. 2013). We investigated the effects of four meteorological variables (precipitation, temperature, solar radiation, and specific humidity) and one morphological variable (LAI) on WUE. Global studies of

the effects of meteorological variables on WUE are rare (Mu et al. 2011b, Ito and Inatomi 2012, Keenan et al. 2013) and there is no consensus on the subject. In a synthetic analysis, Keenan et al. (2013) investigated the inherent WUE (WUEi, WUE multiplied by VPD) using observed GPP and ET data from forest sites in northeast US and Western Europe. They observed an increase in forest WUEi over a period from around the mid-1990s to the present. Despite the slightly different time period, this is consistent with our result for the increasing trend in those areas (Fig. 7a). Keenan et al. (2013) attributed the increases in the WUEi for these forest sites to increasing atmospheric CO_2 concentrations, with a small fraction explained by meteorological or morphological variables. However, Figs. A1–A4 show that the sites Keenan et al. (2013) selected are mainly located within areas where meteorological variables are not changing significantly, i.e., in regions in northeast US and Western Europe.

To further explore how meteorological vari-

ables influence WUE, we assessed how WUE responds to extreme weather events by taking the European droughts during 2000–2010 as an example. Three droughts occurred during this period, i.e., in 2003, 2008 and 2010 (Ivits et al. 2014). We compared WUE in 2010 and that for the averaged values during 2000–2013 (ΔWUE) for the region. During the 2010 European drought, 71% of the area shows a decreased WUE (ΔWUE < 0; Fig. 11a). The averaged WUE was observed to drop for all the three droughts and was most obvious in 2010 (Fig. 11b). All of the biomes show decreased WUE except for OSH in Norway and grasslands of the Alps during this drought (data not shown).

Few studies have examined the effects of LAI on WUE (Hu et al. 2008, Keenan et al. 2013), since most of the studies on WUE have focused on short time periods (usually half an hour or several weeks). However, over longer periods (e.g., seasonal and interannual), LAI could be important in WUE because it can substantially influence WUE by affecting the ratio of transpiration to ET (Hu et al. 2008). WUE increases almost linearly as LAI increases for regions where the LAI is smaller than 1.5 m^2/m^2, whereas WUE does not fluctuate much for regions with LAI larger than 2 m^2/m^2 (Fig. 5). The saturation of WUE with LAI is in agreement with Beer et al. (2009), who calculated WUEi using observed flux datasets. The LAI affects WUE by regulating the ratio of plant transpiration to ET (Hu et al. 2008, Huang et al. 2010). It should be noted that the positive relationship between WUE and LAI may also be partly due to the inherent relationship among the MODIS GPP, ET and LAI datasets, which are derived from the same MODIS reflectance data and ancillary land classification data.

Uncertainty and limitations

Our WUE values are calculated from the MODIS GPP and ET. The MODIS GPP and ET products have significant uncertainty (Zhao et al. 2006, Mu et al. 2011b). MODIS GPP is calculated using a simple multi-product formula (Eq. 1), and the GPP estimates highly depend on the input parameters, especially ε_{max} (maximum light use efficiency). For example, ε_{max} is held constant for each vegetation type in the MODIS GPP algorithm although this parameter is in fact

highly variable (Turner et al. 2006). Other uncertainties may arise from the meteorological inputs from coarser resolutions (Global T62 Gaussian grid, ~1.88° × 1.88° for WGS-84 projection) compared with other MODIS products (Zhao et al. 2006). Similarly, uncertainties of MODIS ET products may arise from the corresponding meteorological inputs, the ET algorithm and other MODIS inputs such as LAI and land cover (Kim et al. 2012, Xue et al. 2013). These uncertainties are indicated in our comparison results (Fig. 1), which show a systematic error of WUE with moderate R^2 (0.55) at the site level. Therefore, this necessitates validation of MODIS products by more measured data and improvement of the algorithm.

Our results show that future work should be conducted to improve the accuracy of MODIS GPP and ET particularly in sparsely vegetated areas. The MODIS GPP and ET products have several sources of uncertainty: model inputs, model structure, and model parameters. For example, the uncertainty in model inputs including meteorological data and the land cover map can lead to significant uncertainty in model simulations (Zhao et al. 2006, Xiao et al. 2011). The uncertainty in model parameters can also lead to significant uncertainty in modeled fluxes (Xiao et al. 2011, 2014). Moreover, the MODIS algorithms for GPP and ET use a single set of parameters to represent each biome and do not consider the spatial heterogeneity within each biome (Eq. 1). In reality, the different physiological parameters may vary even within a given vegetation type because of the variability in soil types, climate and vegetation (Quesada et al. 2010), leading to biases in GPP and ET estimates at the global scale (Castanho et al. 2013). Parameter variability within a vegetation type can lead to large variability in flux estimates (Xiao et al. 2011).

Furthermore, because of the limited data available from the MODIS products, we investigated the temporal trends in WUE for only 14 years. An inter-comparison with WUE from other sources (i.e., IBIS model results and Jung et al. [2011]) show that the MODIS products can detect the disturbances and general trends over the global scale; whereas, absolute values of WUE do not have a consensus among the three datasets. Therefore, a longer time series of WUE
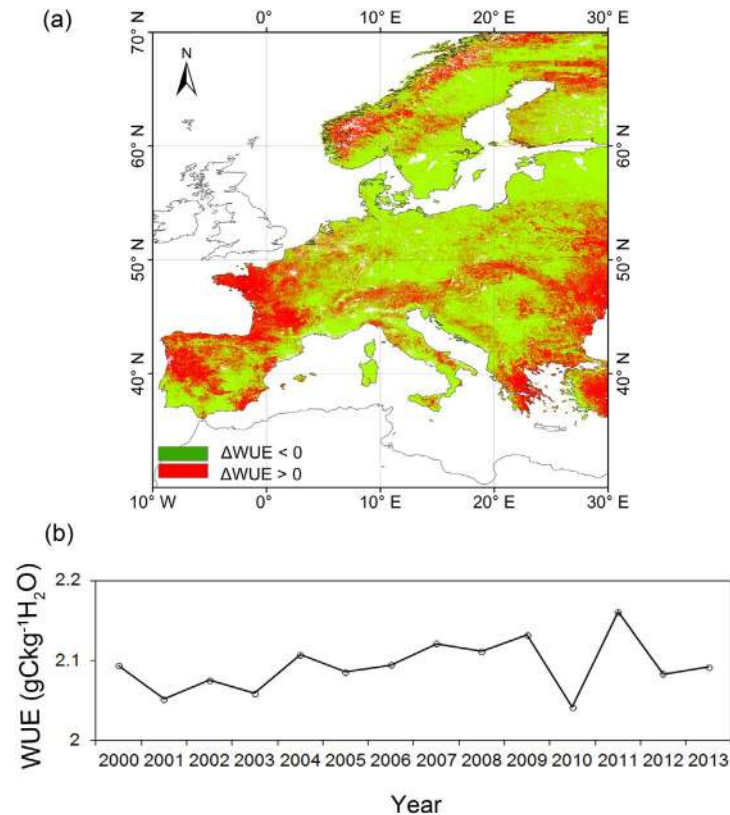
Fig. 11. (a) Spatial patterns of ΔWUE (WUE in 2010 minus averaged WUE for 2000–2013) during European drought of 2010; (b) temporal trends of European averaged WUE for 2000–2013.

values would be even more helpful for understanding vegetation adaption to climate change.

Finally, in this study, we focus on the influences of latitude, altitude, LAI, and four meteorological variables, but WUE could be influenced by other factors such as nutrient cycling (e.g., Keenan et al. 2013), CO_2 concentration (e.g., Saurer et al. 2004, Keenan et al. 2013), and land use change (e.g., Tian et al. 2011), especially over longer time periods. These factors should be considered in future studies when longer time series of WUE and spatially explicit information on these variables become available.

CONCLUSIONS

WUE is an essential parameter that characterizes the coupling of vegetation carbon and water cycles. As a first thorough investigation, this research maps the spatiotemporal patterns of WUE on the global scale. WUE shows large spatial variability globally and is influenced by various meteorological and morphological variables. The WUE also shows a significant increasing trend for most vegetated areas over the study period. The meteorological variables play an important role in temporal variations in WUE. Despite the limitations of the MODIS products, they are perhaps the best gridded data products available for calculating WUE at the global scale. Our results can improve our understanding of the linkages between the global water and carbon cycles by assessing the responses of WUE to climate; and therefore have implications such as future response projection and ecosystem management.

ACKNOWLEDGMENTS

Literature Cited

Baldocchi, D. D. 2003. Assessing the eddy covariance technique for evaluating carbon dioxide exchange rates of ecosystems: past, present and future. Global Change Biology 9:479–492.

Baldocchi, D. D. 2008. 'Breathing' of the terrestrial biosphere: lessons learned from a global network of carbon dioxide flux measurement systems. Australian Journal of Botany 56:1–26.

Beer, C., et al. 2009. Temporal and among-site variability of inherent water use efficiency at the ecosystem level. Global Biogeochemical Cycles 23:GB2018.

Brümmer, C., et al. 2012. How climate and vegetation type influence evapotranspiration and water use efficiency in Canadian forest, peatland and grassland ecosystems. Agricultural and Forest Meteorology 153:14–30.

Castanho, A. D. A., M. T. Coe, M. H. Costa, Y. Malhi, D. Galbraith, and C. A. Quesada. 2013. Improving simulated Amazon forest biomass and productivity by including spatial variation in biophysical parameters. Biogeosciences 10:2255–2272.

Cowan, I. 2002. Fit, fitter, fittest; Where does optimisation fit in? Silva Fennica 36:745–754.

Dan, L. I., and J. Ji. 2007. The surface energy, water, carbon flux and their intercorrelated seasonality in a global climate-vegetation coupled model. Tellus Series B: Chemical and Physical Meteorology 59:425–438.

Desai, A. R., A. D. Richardson, A. M. Moffat, J. Kattge, D. Y. Hollinger, A. Barr, E. Falge, A. Noormets, D. Papale, M. Reichstein, and V. J. Stauch. 2008. Cross-site evaluation of eddy covariance GPP and RE decomposition techniques. Agricultural and Forest Meteorology 148:821–838.

Farquhar, G. D., K. T. Hubick, A. G. Condon, and R. A. Richards. 1989. Carbon isotope fractionation and plant water-use efficiency. Pages 21–40 in P. W. Rundel, J. R. Ehleringer, and K. A. Nagy, editors. Stable isotopes in ecological research. Ecological Studies. Springer, New York, New York, USA.

Friedl, M. A., D. Sulla-Menashe, B. Tan, A. Schneider, N. Ramankutty, A. Sibley, and X. Huang. 2010. MODIS Collection 5 global land cover: algorithm refinements and characterization of new datasets. Remote Sensing of Environment 114:168–182.

Heinsch, F. A., M. Reeves, P. Votava, C. Milesi, M. Zhao, J. Glassy, W. M. Jolly, R. A. Loehman, C. F. Bowker, J. S. Kimball, R. Nemani, and S. W. Running. 2003. User's guide, GPP and NPP (MOD17A2/A3) products. NASA MODIS land algorithms, version 2.0.

Hu, Z., G. Yu, Y. Fu, X. Sun, Y. Li, P. Shi, Y. Wang, and Z. Zheng. 2008. Effects of vegetation control on ecosystem water use efficiency within and among four grassland ecosystems in China. Global Change Biology 14:1609–1619.

Huang, X., Y. Hao, Y. Wang, X. Cui, X. Mo, and X. Zhou. 2010. Partitioning of evapotranspiration and its relation to carbon dioxide fluxes in Inner Mongolia steppe. Journal of Arid Environments 74:1616–1623.

Ito, A., and M. Inatomi. 2012. Water-use efficiency of the terrestrial biosphere: a model analysis focusing on interactions between the global carbon and water cycles. Journal of Hydrometeorology 13:681–694.

Ivits, E., S. Horion, R. Fensholt, and M. Cherlet. 2014. Drought footprint on European ecosystems between 1999 and 2010 assessed by remotely sensed vegetation phenology and productivity. Global Change Biology 20:581–593.

Jin, Y., C. B. Schaaf, C. E. Woodcock, F. Gao, X. Li, A. H. Strahler, W. Lucht, and S. Liang. 2003. Consistency of MODIS surface bidirectional reflectance distribution function and albedo retrievals: 2. Validation. Journal of Geophysical Research: Atmospheres 108:4159.

Jung, M., et al. 2011. Global patterns of land-atmosphere fluxes of carbon dioxide, latent heat, and sensible heat derived from eddy covariance, satellite, and meteorological observations. Journal of Geophysical Research: Biogeosciences 116:G00J07.

Kanamitsu, M., W. Ebisuzaki, J. Woollen, S.-K. Yang, J. J. Hnilo, M. Fiorino, and G. L. Potter. 2002. NCEP–DOE AMIP-II reanalysis (R-2). Bulletin Of The American Meteorological Society 83:1631–1643.

Keenan, T. F., D. Y. Hollinger, G. Bohrer, D. Dragoni, J. W. Munger, H. P. Schmid, and A. D. Richardson. 2013. Increase in forest water-use efficiency as atmospheric carbon dioxide concentrations rise. Nature 499:324–327.

Kim, H., K. Hwang, Q. Mu, S. Lee, and M. Choi. 2012. Validation of MODIS 16 global terrestrial evapotranspiration products in various climates and land cover types in Asia. KSCE Journal of Civil Engineering 16:229–238.

Krishnan, P., T. A. Black, N. J. Grant, A. G. Barr, E. H. Hogg, R. S. Jassal, and K. Morgenstern. 2006.

Impact of changing soil moisture distribution on net ecosystem productivity of a boreal aspen forest during and following drought. Agricultural and Forest Meteorology 139:208–223.

Kucharik, C. J., J. A. Foley, C. Delire, V. A. Fisher, M. T. Coe, J. D. Lenters, C. Young-Molling, N. Ramankutty, J. M. Norman, and S. T. Gower. 2000. Testing the performance of a dynamic global ecosystem model: water balance, carbon balance, and vegetation structure. Global Biogeochemical Cycles 14:795–825.

Law, B. E., et al. 2002. Environmental controls over carbon dioxide and water vapor exchange of terrestrial vegetation. Agricultural and Forest Meteorology 113:97–120.

Linderson, M. L., T. N. Mikkelsen, A. Ibrom, A. Lindroth, H. Ro-Poulsen, and K. Pilegaard. 2012. Up-scaling of water use efficiency from leaf to canopy as based on leaf gas exchange relationships and the modeled in-canopy light distribution. Agricultural and Forest Meteorology 152:201–211.

Lu, X., and Q. Zhuang. 2010. Evaluating evapotranspiration and water-use efficiency of terrestrial ecosystems in the conterminous United States using MODIS and AmeriFlux data. Remote Sensing of Environment 114:1924–1939.

Monteith, J. I. 1964. Evaporation and environment. Pages 205–234 in The state and movement of water in living organisms. Proceeding of the 19th Symposium of the Society for Experimental Biology. Academic Press, New York, New York, USA.

Morén, A. S., A. Lindroth, and A. Grelle. 2001. Water-use efficiency as a means of modelling net assimilation in boreal forests. Trees 15:67–74.

Mu, Q., F. A. Heinsch, M. Zhao, and S. W. Running. 2007. Development of a global evapotranspiration algorithm based on MODIS and global meteorology data. Remote Sensing of Environment 111:519–536.

Mu, Q., M. Zhao, and S. W. Running. 2011a. Evolution of hydrological and carbon cycles under a changing climate. Hydrological Processes 25:4093–4102.

Mu, Q., M. Zhao, and S. W. Running. 2011b. Improvements to a MODIS global terrestrial evapotranspiration algorithm. Remote Sensing of Environment 115:1781–1800.

Myneni, R. B., R. Ramakrishna, R. Nemani, and S. W. Running. 1997. Estimation of global leaf area index and absorbed par using radiative transfer models. IEEE Transactions on Geoscience and Remote Sensing 35:1380–1393.

Niu, S., X. Xing, Z. H. E. Zhang, J. Xia, X. Zhou, B. Song, L. Li, and S. Wan. 2011. Water-use efficiency in response to climate change: from leaf to ecosystem in a temperate steppe. Global Change Biology 17:1073–1082.

Quesada, C. A., et al. 2010. Variations in chemical and physical properties of Amazon forest soils in relation to their genesis. Biogeosciences 7:1515–1541.

Reichstein, M., et al. 2007. Reduction of ecosystem productivity and respiration during the European summer 2003 climate anomaly: a joint flux tower, remote sensing and modelling analysis. Global Change Biology 13:634–651.

Running, S. W., R. R. Nemani, F. A. Heinsch, M. Zhao, M. Reeves, and H. Hashimoto. 2004. A continuous satellite-derived measure of global terrestrial primary production. BioScience 54:547–560.

Salomon, J. G., C. B. Schaaf, A. H. Strahler, G. Feng, and J. Yufang. 2006. Validation of the MODIS bidirectional reflectance distribution function and albedo retrievals using combined observations from the aqua and terra platforms. IEEE Transactions on Geoscience and Remote Sensing 44:1555–1565.

Saurer, M., R. T. W. Siegwolf, and F. H. Schweingruber. 2004. Carbon isotope discrimination indicates improving water-use efficiency of trees in northern Eurasia over the last 100 years. Global Change Biology 10:2109–2120.

Scanlon, T. M., and J. D. Albertson. 2004. Canopy scale measurements of CO_2 and water vapor exchange along a precipitation gradient in southern Africa. Global Change Biology 10:329–341.

Tang, J., P. V. Bolstad, B. E. Ewers, A. R. Desai, K. J. Davis, and E. V. Carey. 2006. Sap flux–upscaled canopy transpiration, stomatal conductance, and water use efficiency in an old growth forest in the Great Lakes region of the United States. Journal of Geophysical Research: Biogeosciences 111:G02009.

Tian, H., G. Chen, M. Liu, C. Zhang, G. Sun, C. Lu, X. Xu, W. Ren, S. Pan, and A. Chappelka. 2010. Model estimates of net primary productivity, evapotranspiration, and water use efficiency in the terrestrial ecosystems of the southern United States during 1895–2007. Forest Ecology and Management 259:1311–1327.

Tian, H., C. Lu, G. Chen, X. Xu, M. Liu, W. Ren, B. Tao, G. Sun, S. Pan, and J. Liu. 2011. Climate and land use controls over terrestrial water use efficiency in monsoon Asia. Ecohydrology 4:322–340.

Turner, D. P., W. D. Ritts, W. B. Cohen, S. T. Gower, S. W. Running, M. Zhao, M. H. Costa, A. A. Kirschbaum, J. M. Ham, S. R. Saleska, and D. E. Ahl. 2006. Evaluation of MODIS NPP and GPP products across multiple biomes. Remote Sensing of Environment 102:282–292.

Van Wijk, M. T., and W. Bouten. 2002. Simulating daily and half-hourly fluxes of forest carbon dioxide and water vapor exchange with a simple model of light and water use. Ecosystems 5:597–610.

Wang, W., J. Xiao, S. V. Ollinger, A. R. Desai, J. Chen, and A. Noormets. 2014. Quantifying the effects of

harvesting on carbon fluxes and stocks in northern temperate forests. Biogeosciences 11:6667–6682.

Xiao, J., K. J. Davis, N. M. Urban, and K. Keller. 2014. Uncertainty in model parameters and regional carbon fluxes: a model-data fusion approach. Agricultural and Forest Meteorology 189–190:175–186.

Xiao, J., K. J. Davis, N. M. Urban, K. Keller, and N. Z. Saliendra. 2011. Upscaling carbon fluxes from towers to the regional scale: Influence of parameter variability and land cover representation on regional flux estimates. Journal of Geophysical Research: Biogeosciences 116:G00J06.

Xiao, J., et al. 2008. Estimation of net ecosystem carbon exchange for the conterminous United States by combining MODIS and AmeriFlux data. Agricultural and Forest Meteorology 148:1827–1847.

Xiao, J., et al. 2013. Carbon fluxes, evapotranspiration, and water use efficiency of terrestrial ecosystems in China. Agricultural and Forest Meteorology 182–183:76–90.

Xue, B.-L., L. Wang, X. Li, K. Yang, D. Chen, and L. Sun. 2013. Evaluation of evapotranspiration estimates for two river basins on the Tibetan Plateau by a water balance method. Journal of Hydrology 492:290–297.

Yang, B. A. I., S. G. Pallardy, T. P. Meyers, L.-H. Gu, P. J. Hanson, S. D. Wullschleger, M. Heuer, K. P. Hos-

man, J. S. Riggs, and D. W. Sluss. 2010. Environmental controls on water use efficiency during severe drought in an Ozark Forest in Missouri, USA. Global Change Biology 16:2252–2271.

Yu, G., X. Song, Q. Wang, Y. Liu, D. Guan, J. Yan, X. Sun, L. Zhang, and X. Wen. 2008. Water-use efficiency of forest ecosystems in eastern China and its relations to climatic variables. New Phytologist 177:927–937.

Zhang, Y., G. Yu, J. Yang, M. C. Wimberly, X. Zhang, J. Tao, Y. Jiang, and J. Zhu. 2013. Climate-driven global changes in carbon use efficiency. Global Ecology and Biogeography 23:144–155.

Zhao, M., F. A. Heinsch, R. R. Nemani, and S. W. Running. 2005. Improvements of the MODIS terrestrial gross and net primary production global data set. Remote Sensing Of Environment 95:164–176.

Zhao, M., and S. W. Running. 2010. Drought-induced reduction in global terrestrial net primary production from 2000 through 2009. Science 329:940–943.

Zhao, M., S. W. Running, and R. R. Nemani. 2006. Sensitivity of Moderate Resolution Imaging Spectroradiometer (MODIS) terrestrial primary production to the accuracy of meteorological reanalyses. Journal of Geophysical Research: Biogeosciences 111:G01002.

SUPPLEMENTAL MATERIAL

ECOLOGICAL ARCHIVES

The Appendix is available online: http://dx.doi.org/10.1890/ES14-00416.1.sm